Auxin-mediated Aux/ IAA-ARF-HB signaling cascade regulates secondary xylem development in Populus

Changzheng Xu, Yun Shen, Fu He, Xiaokang Fu, Hong Yu, Wanxiang Lu, Yongli Li, Chaofeng Li, Di Fan, Hua Cassan Wang, et al.

New Phytologist

Research

Auxin-mediated Aux/IAA-ARF-HB signaling cascade regulates secondary xylem development in *Populus*

Changzheng Xu[1]*, Yun Shen[1]*, Fu He[1]*, Xiaokang Fu[1]*, Hong Yu[1,2]*, Wanxiang Lu[1], Yongli Li[1], Chaofeng Li[1,3], Di Fan[1], Hua Cassan Wang[4] and Keming Luo[1]

[1]Chongqing Key Laboratory of Plant Resource Conservation and Germplasm Innovation, School of Life Sciences, Southwest University, Chongqing 400715, China; [2]School of Basic Medical Sciences, Southwest Medical University, Luzhou, Sichuan 646000, China; [3]Key Laboratory of Adaptation and Evolution of Plateau Biota, Northwest Institute of Plateau Biology, Chinese Academy of Sciences, Xining 810008, China; [4]UMR5546, Laboratoire de Recherche en Sciences Végétales, Université de Toulouse III Paul Sabatier, CNRS, UPS, 31326, Castanet-Tolosan, France

Authors for correspondence:
Hua Cassan Wang
Tel: +33 5 34323851
Email: huawang76@yahoo.com

Keming Luo
Tel: +86 23 68253021
Email: kemingl@swu.edu.cn

Received: *13 November 2018*
Accepted: *14 December 2018*

New Phytologist (2019)
doi: 10.1111/nph.15658

Key words: ARF5, Aux/IAA9, auxin, HD-ZIP III transcription factors, *Populus*, xylem development.

Summary

- Wood development is strictly regulated by various phytohormones and auxin plays a central regulatory role in this process. However, how the auxin signaling is transducted in developing secondary xylem during wood formation in tree species remains unclear.
- Here, we identified an Aux/INDOLE-3-ACETIC ACID 9 (IAA9)-AUXIN RESPONSE FACTOR 5 (ARF5) module in *Populus tomentosa* as a key mediator of auxin signaling to control early developing xylem development.
- *PtoIAA9*, a canonical *Aux/IAA* gene, is predominantly expressed in vascular cambium and developing secondary xylem and induced by exogenous auxin. Overexpression of *PtoIAA9m* encoding a stabilized IAA9 protein significantly represses secondary xylem development in transgenic poplar. We further showed that PtoIAA9 interacts with PtoARF5 homologs via the C-terminal III/IV domains. The truncated PtoARF5.1 protein without the III/IV domains rescued defective phenotypes caused by *PtoIAA9m*. Expression analysis showed that the PtoIAA9-PtoARF5 module regulated the expression of genes associated with secondary vascular development in *PtoIAA9m*- and *PtoARF5.1*-overexpressing plants. Furthermore, PtoARF5.1 could bind to the promoters of two Class III homeodomain-leucine zipper (HD-ZIP III) genes, *PtoHB7* and *PtoHB8*, to modulate secondary xylem formation.
- Taken together, our results suggest that the Aux/IAA9-ARF5 module is required for auxin signaling to regulate wood formation via orchestrating the expression of HD-ZIP III transcription factors in poplar.

Introduction

Meristems, specialized structures of reservoirs of stem cells undergoing proliferation, drive postembryonic developmental programs in plants (Nakajima & Benfey, 2002). In comparison with primary/longitudinal growth of shoots and roots mediated by apex-localized meristems, secondary/radial growth is dominated by vascular cambium (Campbell & Turner, 2017). Cambial cells sequentially undergo proliferation and differentiation into secondary vascular tissues (Matte Risopatron *et al.*, 2010). Different from herbaceous plants, trees exhibit perennial stem thickening during their life cycle due to continuous competence of the vascular cambium (Sanchez *et al.*, 2012). The secondary xylem, commonly called wood, overwhelmingly contributes to stem thickening of trees (Sanchez *et al.*, 2012). Wood production is a predominant proportion of biomass accumulation in terrestrial ecosystems and is also of outstanding economic value (Ragauskas *et al.*, 2006; Bonan, 2008).

Cambium-originated wood formation starts with specification of secondary xylem cell precursors, which in turn undergo a series of cellular events for maturation, including expansion, secondary cell-wall deposition and programmed cell death (Ye & Zhong, 2015). Cambial homeostasis between stem cell identity and xylem specification affects the deposition of xylem cell layers (Campbell & Turner, 2017). Expansion of newly specified xylem cells contributes to the size of woody elements, while secondary wall deposition is important for functional maturation of xylem. Although vessels and fibers are lignified components of secondary xylem, they differ in cell size, secondary cell-wall deposition and cell viability (Fukuda, 2004). These differences result from the cellular changes in cytoskeletal arrangement, secondary wall patterning and autolysis that occur during differentiation of tracheary elements, the unit of xylem vessels (Fukuda, 2004; Turner *et al.*, 2007). These coordinated behaviors of cambial cells and

*These authors contributed equally to this work.

their differentiating descendants are intricately and dynamically orchestrated by various genetic and environmental factors (Dejardin *et al.*, 2010; Ye & Zhong, 2015). Recent high-spatial-resolution profiling analyses in *Populus* have revealed three transcriptome reprogramming events coinciding with transitions of distinct cellular behaviors in the context of wood formation (Sundell *et al.*, 2017). Although a comprehensive picture of the gene regulatory machinery involved in secondary growth has emerged in recent decades, precise regulation of spatially organized and temporally coordinated cellular events for wood differentiation remains largely unknown.

Auxin is a crucial phytohormone for cell–cell communication in meristems (Leyser, 2005). Auxin signaling is able to direct cellular behaviors, including cell division, expansion and differentiation, for various developmental programs (Vanneste & Friml, 2009; Perrot-Rechenmann, 2010). Previous studies have shown that auxin accumulates in a radial gradient pattern across wood-forming tissues with a peak in concentration in cambium and bilateral decay towards differentiating secondary xylem and phloem (Tuominen *et al.*, 1997; Uggla *et al.*, 1998; Immanen *et al.*, 2016). Auxin is thus considered as a primary regulator of secondary xylem formation in a morphogen-like manner (Uggla *et al.*, 1996; Sundberg *et al.*, 2000). In *Pinus*, a lack of auxin supply from shoot apex leads to a loss of fusiform shape of cambial derivatives (Savidge, 1983). Introduction of a stabilized version of PttIAA3 (homolog of IAA20s in Arabidopsis and *Populus*; Supporting Information Fig. S1) that represses auxin response in hybrid aspen attenuates periclinal division of cambial cells, but enhances stem cell characteristics as indicated by an enlarged zone of anticlinal cell division in cambium (Nilsson *et al.*, 2008). These findings reveal a dual role of auxin in coordinating cambial identity and proliferation activity. Recently, detection of auxin signaling via a high-affinity sensor indicates its moderate level in cambial stem cells, while increased level in differentiating cambial descendants (Brackmann *et al.*, 2018). These results implicate the key role of auxin signaling in cambial differentiation. Consistently, exogenous auxin is able to induce differentiation of intact and functionally normal secondary xylem cells (Björklund *et al.*, 2007). Local enhancement of auxin signaling is required for wood formation, also supporting the action of auxin in recruiting cells for differentiation (Bargmann *et al.*, 2013; Muller *et al.*, 2016). However, the precise regulation of auxin signaling on these coordinated cellular events for wood differentiation remains obscure in trees.

Auxin perception starts with auxin binding to TIR1 (TRANSPORT INHIBITOR RESPONSE1)/AFB (AUXIN SIGNALING F-BOX) receptors, and leads to subsequent degradation of the Aux/IAA proteins that repress auxin signaling via physical interactions with auxin response factor (ARF) proteins (Mockaitis & Estelle, 2008). The auxin-stimulated protein turnover of Aux/IAAs releases the transcriptional activity of their partner ARFs to activate downstream auxin responsive gene expression (Vanneste & Friml, 2009). Different Aux/IAA-ARF modules are known to regulate corresponding auxin-responsive genes and developmental processes (Vanneste & Friml, 2009). In Arabidopsis, the IAA12/BODENLOS (BDL)-ARF5/MONOPTEROS (MP) module was identified to control provascular specification and patterning during embryogenesis (Hardtke & Berleth, 1998; Hamann *et al.*, 2002). ARF5/MP is also crucial for leaf (pre)procambial specification during leaf vein patterning (Przemeck *et al.*, 1996). In hybrid aspen, eight *Aux/IAA* members were assayed for expression of auxin responsive genes in wood tissues and during transitions of cambial activity (Moyle *et al.*, 2002), and *PttIAA3* was identified as an important mediator of auxin-dependent regulation of cambial proliferation activity (Nilsson *et al.*, 2008). When a *Eucalyptus* Aux/IAA member *IAA4* (*EgrIAA4*) was ectopically expressed in Arabidopsis, secondary xylem formation of the transgenic plants was dramatically reduced (Yu *et al.*, 2015).

Various plant model systems have been used to study the mechanisms governing plant vascular development. The construction of genetic networks underlying vascular tissue specification has been mainly achieved based on research on four organs/systems: provascular specification during embryogenesis, procambial cell specification during root development (primary growth), (pre)procambial cell specification during leaf vein patterning (primary growth), and cambium specification during secondary growth in stem for wood formation (Campbell & Turner, 2017). For embryogenesis and procambial specification during primary growth in roots and leaf veins, the key components of auxin signaling have been identified: the IAA12/BDL-ARF5/MP module for embryogenesis (Hardtke & Berleth, 1998; Hamann *et al.*, 2002), the ARF5/MP-mediated pathway for leaf vein patterning (Przemeck *et al.*, 1996; Donner *et al.*, 2009), and the IAA20/IAA30-ARF5/MP combinations for root development (Muller *et al.*, 2016). To date, however, it remains unknown which Aux/IAA-ARF combination mediates auxin-dependent cambial specification of secondary growth for wood formation.

Here, we identified *PtoIAA9* as a novel key component in modulating wood formation in *Populus tomentosa*. Functional characterization of the PtoIAA9–PtoARF5 module revealed auxin-dependent differentiation of secondary xylem derived from the cambium, and demonstrated their roles in orchestrating xylem cell specification, woody cell size and vessel density. Moreover, we provided biochemical and genetic evidence that *PtoHB7* and *PtoHB8*, encoding HD-ZIP III transcription factors, are direct targets of the PtoIAA9–PtoARF5 module to coordinate cellular behaviors associated with woody cell differentiation. Our results provide novel insights into auxin-dependent regulation on the dynamic and coordinated cellular events for secondary xylem differentiation in woody species.

Materials and Methods

Gene cloning and plasmid construction

The full-length coding sequence of *PtoIAA9*, *PtoARF5.1* and *PtoARF5.2* was amplified from cDNA of *P. tomentosa* using gene-specific primer pairs (Table S1), and constructed into the pCXSN vector (Chen *et al.*, 2009), respectively. To substitute the first proline (P) with serine (S) within the Degron motif, overlap PCR was performed using pCXSN-*PtoIAA9* as templates. The resulting PCR product was ligated into pCXSN under control of

the *CaMV 35S* promoter to generate the plasmid for overexpressing *PtoIAA9m*. The full-length sequence of *PtoARF5.1* was subcloned into the modified pCAMBIA1305 with a kanamycin resistant gene. The sequence of *PtoARF5.1Δ* harboring the N-terminal 1995 nucleotides of *PtoARF5.1* was amplified from pCXSN-*PtoARF5.1* and constructed into the modified pCAMBIA1305 vector. A 2-kb promoter fragment upstream of *PtoIAA9* was amplified from genomic DNA of *P. tomentosa* using the primer pair *Pro-PtoIAA9*-fw/rv (Table S1), and inserted into pXGUS-P to drive the *GUS* reporter gene (Chen *et al.*, 2009).

Genetic transformation and growth conditions

P. tomentosa was stably transformed using the method of *Agrobacterium*-mediated infiltration of leaf disks as described previously (Jia *et al.*, 2010). PCR genotyping with the primers of hygromycin/kanamycin-resistant genes was performed for the identification of positive transgenic plants. Transgenic and WT poplar plants were propagated via *in vitro* microcutting. For clonal propagation, shoot segments of 3–4 cm with two or three young leaves were cut from sterilized seedlings and cultivated on woody plant medium solid medium at 25°C with 16 h light of 5000 lux and 8 h dark. For phenotype analyses, 4-wk-old microcutting-propagated seedlings were transferred to soil in pots, and cultivated in a glasshouse at 23–25°C with the light of 10 000 lux under a 16 h: 8 h, day : night cycle.

Cross-sectioning and histological staining

The 7th internodes were sectioned with a razor blade, and then stained with 0.05% (w/v) toluidine blue for 5 min. The cross-sections were observed and captured using a microscope (Zeiss). The images were analyzed using ImageJ (https://imagej.nih.gov/ij/) for quantifying morphological parameters of xylem cells.

RNA *in situ* hybridization

For probe preparation, 276- and 223-bp gene-specific cDNA fragments were amplified for *PtoIAA9* and *PtoARF5.1*, respectively (Table S1). The two probes were labeled using a DIG RNA Labeling Kit (Roche). Section pretreatment, hybridization and immunological detection were performed as previously described (Sang *et al.*, 2012).

GUS staining

For GUS staining (Jefferson, 1987), cross-sections of the 7th internodes of 2-month-old plants were fixed in acetone for 1 h at −20°C, and then washed twice in double distilled H_2O (ddH_2O). The cross-sections were soaked in GUS staining solution (0.5 M Tris, pH 7.0, 10% Triton X-100 with 1 mM X-Gluc (5-bromo-4-chloro-3-indolyl-D-glucuronide)) for 15 min at 37°C in the dark. After reaction, Chl was removed by use of 75% ethanol three times at 65°C. The Chl-free stained stems were observed under an Olympus 566 SZX16 microscope (Tokyo, Japan) and documented using an Olympus DP73 camera.

qRT-PCR

Total RNA was extracted from tissues of 2-month-old *P. tomentosa* plants using a Plant RNeasy Mini Kit (Qiagen). cDNA was synthesized using a PrimeScript™ RT reagent Kit with gDNA Eraser (Takara, Dalian, China). Quantitative real time polymerase chain reaction (qRT-PCR) was performed using SYBR Premix ExTaqTM (Takara) in a TP800 Real-Time PCR machine (Takara). The poplar *18S rRNA* gene was used as the reference gene as an internal standard. The primers used for qRT-PCR are listed in Table S1.

Transactivation test in yeast

The recombinant plasmids were introduced into the yeast strain *Saccharomyces cerevisiae* Gold2 using the PEG/LiAC method. The transformed strains were screened on synthetic dropout (SD medium) lacking tryptophan (Trp; SD/-T) for selection of positive clones. Subsequently, positive clones were transferred to SD medium lacking Trp, histidine (His) and adenine (Ade; SD/-ATH) and cultivated at 28°C for 2 d. Positive clones were used for transactivation analysis on X-α-gal indicator plates. A digital camera (EOS 550D, Canon, Tokyo, Japan) was used to photograph yeast cells.

Yeast two-hybrid (Y2H) assays

Y2H assays were performed based on the manufacturer's instructions (Clontech, Palo Alto, CA, USA). The AD and BD fusion constructs were co-transformed into yeast strain Gold2 as described above. The transformants were screened on SD medium lacking tryptophan (Trp) and leucine (Leu; SD/-TL) at 28°C. After 3 d, positive clones were cultured in YPD liquid medium for 1 d to an OD_{600} of 1.0, and the yeast solution was diluted with ddH_2O to 1–10^3x, and then transferred to SD medium lacking Trp, Leu, histidine (His) and adenine (Ade; SD/-AHTL) and cultured for 2 d. A EOS 550D digital camera was used to photograph yeast cells.

Bimolecular fluorescence complementation (BiFC)

For BiFC assays, full-length coding sequences of *PtoIAA9* and *PtoARF5.1* were cloned from pCXSN-*PtoIAA9* and pCXSN-*PtoARF5.1*, and ligated into pXY104 and pXY106 vectors, respectively. The vectors pXY104 and pXY106 carrying the N- and C-terminal halves of yellow fluorescent protein (YFP) were used. The open reading frame (ORF) of *PtoIAA9* was cloned into pXY106, while that of PtoARF5.1 was constructed into pXY104. The constructs were co-transformed into tobacco as described above, and observed by confocal laser microscopy (Olympus 589 FV1200).

Chromatin immunoprecipitation (ChIP) assay

ChIP analysis was performed as previously described (Yang *et al.*, 2012). One-month-old *PtoARF5.1* transgenic poplar plants

harboring the HA epitope were used as samples; the HA antibody and normal mouse IgG were used for immunoreaction. All primers used in ChIP assays are listed in Table S1.

Effector-reporter test

Promoters of the *PtoHB7* and *PtoHB8* genes were amplified via specific primers (Table S1) and constructed into pCXGUS-P. The *35S:PtoARF5.1* and *35S:PtoARF5.1Δ* vectors were used as effectors. Tobacco leaves were transformed by *Agrobacteria* containing the effectors and reporters as described above. After 3 d of infiltration, GUS activity was measured by monitoring the cleavage of 4-methyl umbelliferyl β-D-glucuronide (MUG), the substrate of β-glucuronidase, which produces the fluorescent 4-methyl umbelliferone (4MU) upon hydrolysis. Protein concentrations were determined via the Bradford method.

Gene accessions

GeneBank accession numbers of the *P. tomentosa* genes are: *PtoIAA9* (MH345700), *PtoARF5.1* (MH352401), *PtoARF5.2* (MH352402) and *PtoHB7* (MH345699).

Results

IAA9 is highly expressed across wood-forming tissues in poplar

A total of 35 *Aux/IAA* genes were previously predicted in the poplar genome (Kalluri *et al.*, 2007). These *Aux/IAA* genes were identified in the more recent release of the *Populus trichocarpa* genome (v3.0; https://phytozome.jgi.doe.gov) and designated according to phylogenetic relationships with their Arabidopsis orthologues (Fig. S1a). To determine the members that play a key role during wood formation, expression levels of all *Aux/IAA* genes were comprehensively evaluated using the high-spatial-resolution RNA sequencing data of the wood-forming tissues in poplar (Sundell *et al.*, 2017). Among them, *IAA9*, *-11*, *-16.1*, *-16.2* and *-29.1* showed high expression (Fig. S1). Continuous assays across secondary xylem tissues in poplar stems (Sundell *et al.*, 2017) allowed us to evaluate spatial expression patterns of these highly expressed *Aux/IAA*s and some other members, such as *IAA12.1*, *-12.2*, *-20.1* and *-20.2* (Fig. S2b). A highly similar expression pattern was shared by *IAA9*, *-16.1* and *-16.2*, extending from the cambium to differentiated xylem (Fig. S2b), which was validated by correlation tests (Pearson correlation coefficient $R^2 = 0.82$ or 0.51, $P < 0.01$; Fig. S2c). For this pattern, the transcripts of these three *Aux/IAA*s accumulated in the cambial zone and developing xylem, and then decreased towards differentiated xylem (Fig. S2d), consistent with the previously reported auxin distribution across wood-forming tissues of poplar stems (Uggla *et al.*, 1998; Immanen *et al.*, 2016). By contrast, *IAA11* and *-29.1* displayed totally different expression patterns (Fig. S2b). Thus, *IAA9*, *-16.1* and *-16.2* were considered key *Aux/IAA* genes of auxin signaling involved in wood formation in poplar. Tissue-specific expression assays by qRT-PCR in *P. tomentosa* further confirmed the enriched transcript abundance of *IAA9*, *-16.1* and *-16.2* in stems (Fig. S2d). We selected *PtoIAA9* from *P. tomentosa* as a candidate gene to further investigate auxin-dependent regulation of wood formation.

To determine the exact expression pattern of *PtoIAA9* in secondary vascular tissues, RNA *in situ* hybridization was performed using the fifth internode of 1.5-month-old poplar (Fig. 1a,b). Transcripts of *PtoIAA9* were preferentially accumulated in the cambial zone and neighboring cells (Fig. 1a). Furthermore, the GUS reporter driven by the *PtoIAA9* promoter in transgenic poplar confirmed its expression in the cambium zone and closely neighboring cell layers of the wood-developing stem (Fig. 1c,d). qRT-PCR assays revealed a more than 3-fold induced transcript abundance of *PtoIAA9* in stems within 3 h of exogenous auxin (Fig. 1e). The auxin-inducible expression was also examined by quantification of GUS activity driven by the *PtoIAA9* promoter in wood-forming tissues (Fig. 1f). These results indicated that *PtoIAA9* is an auxin-inducible gene predominantly expressed in cambium and adjacent cells towards xylem differentiation.

PtoIAA9 encodes a canonical Aux/IAA protein belonging to a distinct clade

PtoIAA9 protein harbors the characteristic domains (Domain I, II, III and IV; Reed, 2001) of Aux/IAAs in high sequence similarity to its close homologs in other plant species (Fig. S3). Remarkably, PtoIAA9 belongs to a distinct clade among all Aux/IAA members due to its 50% longer amino acid sequence (*c.* 300 aa) compared with the average length (*c.* 200 aa) of other Aux/IAA members (Wang *et al.*, 2005). Transient expression of a *PtoIAA9-GFP* fusion gene revealed that PtoIAA9 is a nucleus-localized protein (Fig. S4a; Methods S1), consistent with the prediction of both bipartite and SV40-type nuclear localization signals (NLS) present within its sequences (Fig. S3). Aux/IAA proteins usually contain a short amino acid stretch (VGWPP) called Degron that confers auxin-stimulated protein turnover (Worley *et al.*, 2000). Due to the presence of a typical Degron motif in its Domain II, auxin-responsive protein stability of PtoIAA9 fused with a green fluorescent protein (GFP) tag was monitored in transiently expressed epidermal cells of tobacco leaves (Fig. S4b; Methods S1). The fluorescent signals of PtoIAA9-GFP were significantly reduced in the leaf epidermal cells subject to IAA (Fig. S4b), as validated by quantifying the percentage of fluorescent nuclei and fluorescence intensity per nucleus (Fig. S4c,d). By contrast, this auxin-induced protein instability disappeared when the first proline (P) within the Degron motif of PtoIAA9 was replaced by serine (S) (ns, not significant; $P > 0.05$; Fig. S4b–e). Moreover, stronger fluorescence was detected in these leaf epidermal cells transiently transformed by the *PtoIAA9* mutant gene with impaired Degron motif, compared to the wild-type control (Fig. S4b–d), indicating that the auxin-inducible rapid turnover of PtoIAA9 depends on its Degron motif. Self-activation assays in yeast showed that PtoIAA9 has no transcriptional activating activity (Fig. S4f). Additionally, PtoIAA9 compromised the activating capability of the VP16 domain, demonstrating that it is a transcriptional repressor. The truncated PtoIAA9 protein without

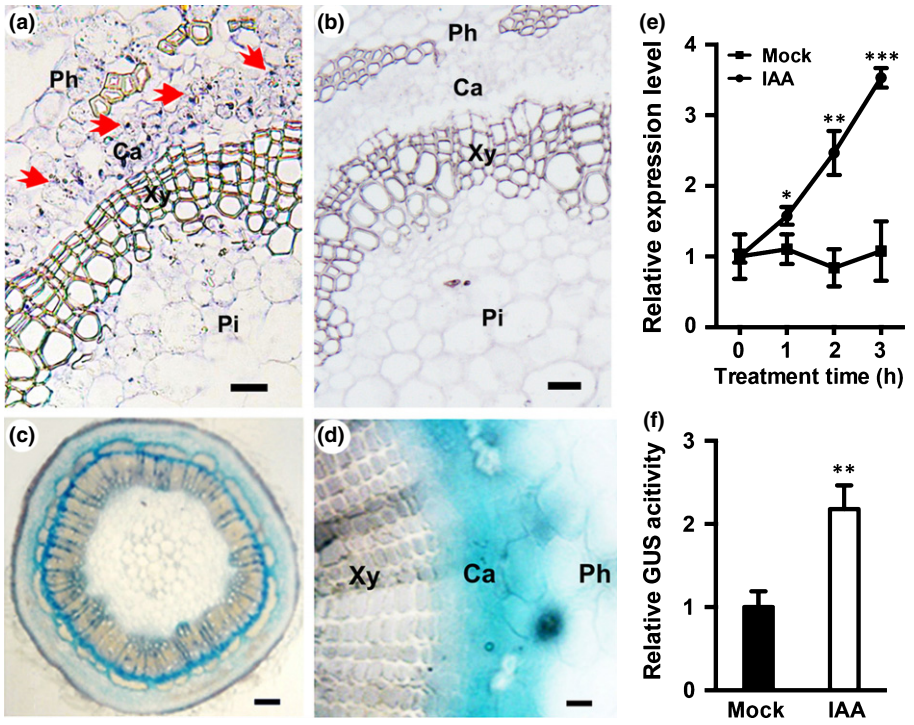

Fig. 1 Expression pattern and auxin induction of *PtoIAA9* transcripts in wood-forming tissues of *Populus tomentosa* stem. (a, b) RNA *in situ* hybridization of *PtoIAA9* in secondary vascular tissues of poplar. The 5th internodes of 1.5-month-old poplar plants cultivated in soil were cross-sectioned for hybridization with antisense (a) and sense (b) probes of *PtoIAA9*. Red triangles indicate *in situ* hybridization signals for *PtoIAA9* transcripts. Ca, cambium; Ph, phloem; Pi, pith; Xy, xylem. (c, d) Histological staining of the GUS reporter driven by the promoter of *PtoIAA9* in poplar stems. The 7th internodes of 1.5-month-old poplar plants cultivated in soil were cross-sectioned for GUS staining. Ca, cambium; Ph, phloem; Xy, xylem.. (e) Time-course assays of auxin-induced transcript abundance of *PtoIAA9* in poplar stems. The microcutting-propagated poplar seedlings cultivated *in vitro* for 4 wk were subjected to 5 μM IAA for 0, 1, 2 and 3 h, and stem tissues were collected for RNA extraction followed by qRT-PCR assays. 18S rRNA was used as a reference gene. Expression levels are indicated relative to values for 0 h (with 0 h set arbitrarily to 1). Error bars represent ± SD. Asterisks indicate significant differences between mock and auxin treatment at each time point (Student's *t* test): *, $P < 0.05$; **, $P < 0.01$; ***, $P < 0.001$; $n = 3$. (f) Quantification of auxin-induced GUS activity driven by the promoter of *PtoIAA9* in poplar stem. IAA treatment (5 μM) was performed for 6 h as indicated in (d). The values under mock treatment were normalized to 1. Error bars represent SD. Asterisks indicate significant differences with respect to mock (Student's *t* test): **, $P < 0.01$; $n = 4$. Bars: (a, b) 200 μm; (c) 500 μm; (d) 100 μm.

Domain I at the C-terminal region (BD-VP16-PtoIAA9t) showed repressing activity (Fig. S4f). Taking this together, PtoIAA9 exhibits molecular features typical of canonical Aux/IAA repressors.

Overexpression of an auxin-resistant *PtoIAA9m* represses wood formation

To identify its role in regulating secondary xylem development during wood formation, the auxin-resistant *PtoIAA9* containing the impaired Degron sequence (Fig. S4e; *PtoIAA9m*) was constitutively expressed in poplar (*PtoIAA9m*-OE; Fig. S5a). Representative overexpressing lines displayed significantly reduced plant growth compared to the wildtype (WT; Fig. 2a). Quantitative measurement revealed that overexpression of *PtoIAA9m* led to a 40–50% reduction in plant height and 35% reduction in stem diameter (Fig. 2b,c). Similar changes were indicated by a time-course analysis of these two parameters (Fig. S5b,c). The internode number of WT and transgenic plants was not changed (ns; $P > 0.05$; Fig. S5d). Secondary vascular tissues were examined in *PtoIAA9m*-OE plants stained with toluidine O (Fig. 2d). Secondary xylem development was significantly repressed by overexpressing *PtoIAA9m* (Fig. 2d), with a 40% decrease in the number of xylem cell layers, compared with WT (Fig. 2e). The percentage of secondary xylem occupying the whole stem was 46.8% in WT, but was attenuated to 39.1% in the *PtoIAA9m*-OE lines, whereas that of phloem was not affected (Fig. 2f). These results indicated that *PtoIAA9m* might inhibit wood formation.

PtoIAA9-attenuated auxin signaling impairs secondary xylem formation

To determine PtoIAA9-dependent regulation of wood formation, we first examined phenotypes of wood-associated cell types, including cambium, xylem fibers and vessels in transgenic poplar. The results showed that cambial cells were arrayed more tightly in *PtoIAA9m*-OE plants than WT (Fig. 2g), but the number of cambial cell layers was not significantly affected by overexpression of *PtoIAA9m* (ns; $P > 0.05$; Fig. S5e). Cross-sections of different internodes in WT revealed the presence of one or two particular cell layers on the side of the cambium zone towards the xylem

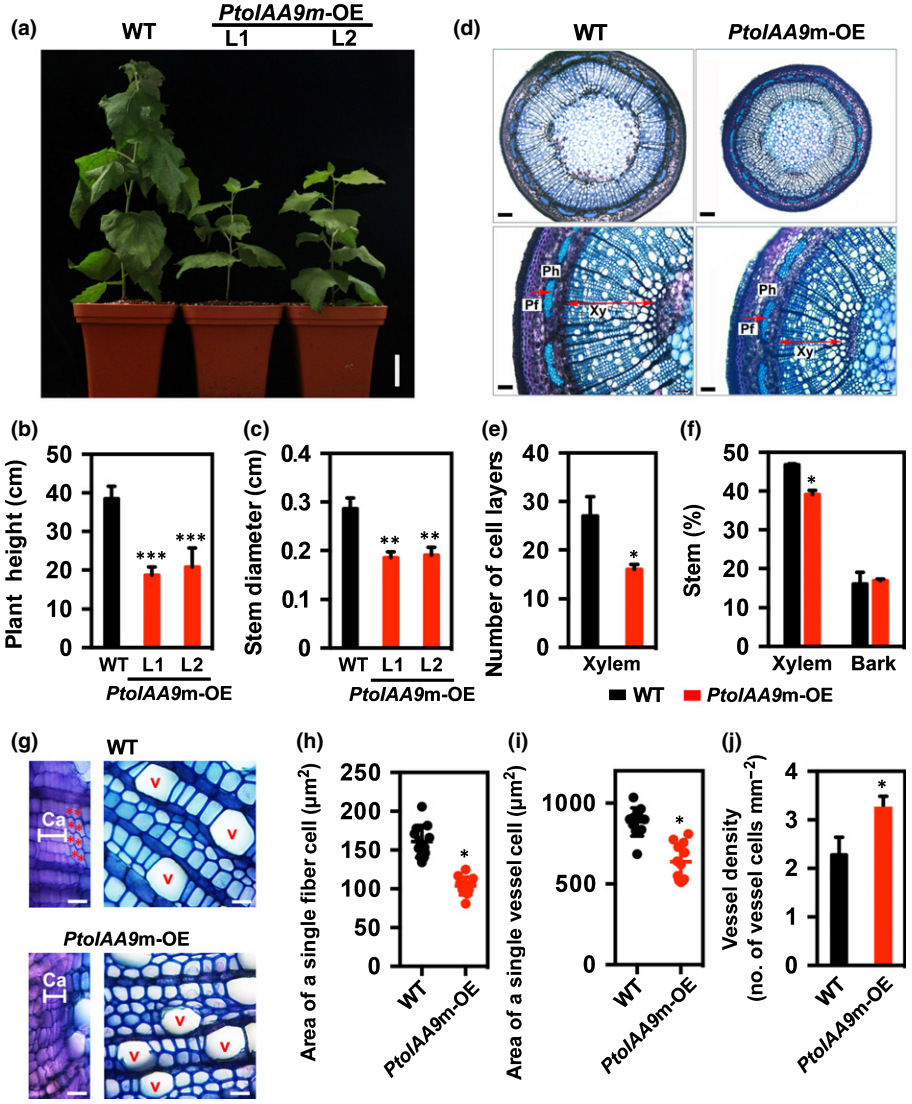

Fig. 2 Wood phenotypes resulting from *PtoIAA9m* overexpression in *Populus tomentosa*. (a) Dwarf phenotypes of 2-month-old plants of independent *PtoIAA9m*-overexpressing (*PtoIAA9m*-OE) transgenic poplar lines (L1 and L2). (b, c) Measurement of plant height (b) and stem diameter (c) of *PtoIAA9m*-OE transgenic poplar lines corresponding to (a). (d) Cross-sectioning and staining with toluidine blue of the 7th internode of 2-month-old wild-type (WT) and *PtoIAA9m*-OE transgenic plants (L1). Ph, phloem; Pf, phloem fibers; Xy, xylem. (e) Quantification of secondary xylem cell layers in WT and *PtoIAA9m*-OE transgenic plants (L1). The number of secondary xylem cell layers was counted in toluidine blue-stained anatomical sections of the 7th internode of WT and *PtoIAA9m*-OE transgenic plants. (f) Percentage of secondary xylem and bark in the stem of WT and *PtoIAA9m*-OE transgenic plants (L1). The area of secondary xylem, bark and total stem was measured via ImageJ in toluidine blue-stained anatomical sections of the 7th internode of WT and *PtoIAA9m*-OE transgenic plants. (g) Detailed observation of the cambial zone and woody cells of secondary xylem in WT and *PtoIAA9m*-OE plants. The images were captured on toluidine blue-stained anatomical sections of the 7th internode of the corresponding lines. White lines indicate cambium (Ca), and red stars represent the cells of early developing xylem (EDX). V, vessel. (h, i) Quantification of the size of a single fiber (h) and vessel (i) cell in stem of WT and *PtoIAA9m*-OE plants. The area of fiber and vessel cells was measured and calculated via ImageJ based on the images of toluidine blue-stained anatomical sections as described in the Materials and Methods section. (j) Density of vessels in stem of WT and *PtoIAA9m*-OE plants. The number of vessels was counted based on the images of toluidine blue-stained anatomical sections. Error bars represent SD. Asterisks indicate significant differences with respect to values of WT (Student *t*-test): *, $P < 0.05$; **, $P < 0.01$; ***, $P < 0.001$; $n = 4$. Bars: (a) 5 cm; (d) upper, 250 μm, lower, 100 μm; (g) 50 μm.

(Figs 2g, S5f). These cells were not stained by toluidine blue, suggesting that lignin deposition was not initiated for secondary cell wall formation. These cells were distinctly larger than cambial cells but smaller than mature xylem cells (Figs 2g, S5f). These features indicated that these cells were newly differentiated from cambium zone towards xylem and undergoing cell expansion, and thereby considered as early developing xylem (EDX). However, these EDX cell layers were greatly reduced and almost absent in cross-sections of *PtoIAA9m*-OE stems (Fig. 2g), resembling EDX cells just before dormancy due to reduced rate of cambium cell periclinal division. This greatly reduced EDX cell layer suggests that overexpression of stabilized PtoIAA9 inhibited the periclinal division of cambium, thus leading to reduced wood formation.

Quantitative measurement showed that the cell size of xylem fibers and vessels was reduced by 36% and 28% in *PtoIAA9m*-OE plants relative to WT (Fig. 2g–i). By contrast, vessel density was significantly increased by 42% in *PtoIAA9m*-OE plants (Fig. 2g,j). Cell wall thickness was not affected by overexpressing *PtoIAA9m* (ns; $P > 0.05$; Fig. S5g). Together, these data suggested that PtoIAA9m inhibited developing xylem cell (vessel and fiber) differentiation and expansion.

PtoIAA9 interacts with PtoARF5s

PtoIAA9 contains intact Domains III and IV (also called PB1 domain) that mediate physical interaction with ARFs, a family of plant-specific B3-type transcription factors directly driving the expression of auxin responsive genes (Vanneste & Friml, 2009). We speculated that PtoIAA9 might interact with ARF proteins to regulate wood formation in poplar. A previous study has shown that ARF5/MP is a key regulator of auxin-dependent vascular patterning during embryogenesis and leaf vein patterning in Arabidopsis (Donner *et al.*, 2009; Brackmann *et al.*, 2018). The poplar genome harbors duplicated *ARF5* members, designated *ARF5.1* and *ARF5.2*, which are expressed in secondary vascular tissues of stems (Johnson & Douglas, 2007). Poplar ARF5s share conserved modular structure with their Arabidopsis homolog containing intact Domains III and IV (Fig. S6a), implying that they may interact with PtoIAA9. To determine the interactions between PtoIAA9 and PtoARF5s, we performed Y2H assay (Fig. 3a). Owing to the presence of the B3 domain with DNA-binding activity, the coding region of PtoARF5s was fused to AD, and the resulting fused protein was subsequently coexpressed in yeast cells with PtoIAA9-BD. Both PtoARF5 paralogs were shown to interact with PtoIAA9, but PtoARF5.1 displayed stronger interaction ability than PtoARF5.2 (Fig. 3a). The PtoIAA9–PtoARF5 interaction was subsequently confirmed by BiFC analyses (Fig. 3b).

Despite the physical interactions, the PtoIAA9–PtoARF5-dependent regulation on wood formation requires their coexpression in secondary vascular tissues. Analysis of expression patterns based on RNAseq datasets (Sundell *et al.*, 2017) revealed the highly correlated transcript accumulation between IAA9 and ARF5s in poplar wood-forming tissues (Fig. S6b,c). Similar to the expression patterns of *PtoIAA9*, RNA *in situ* hybridization results showed that *PtoARF5.1* was highly expressed in developing wood-associated tissues of poplar (Fig. 3c,d).

PtoARF5.1 rescues *PtoIAA9m*-affected secondary xylem differentiation

Physical interactions and overlapping expression of *PtoIAA9* and *PtoARF5*s suggested their cooperative involvement in the regulation of wood formation. To test this hypothesis, functional complementation of *PtoARF5.1* was performed on *PtoIAA9m*-OE-resulting phenotypes of secondary xylem development (Fig. 4). To avoid the undesirable effects of *PtoIAA9* overexpression and other endogenous *Aux/IAA* genes on its function, a full-length *PtoARF5.1* and a truncated form without C-terminal Domains III and IV responsible for Aux/IAA interactions (*PtoARF5.1Δ*) were introduced into the *PtoIAA9m*-OE transgenic lines, respectively (Figs 4, S6). Y2H tests showed that the C-terminal deletion abolished the interactions of PtoARF5.1 with the PtoIAA9 protein (Fig. S7a), but did not affect transcriptional activation (Fig. S7b).

Phenotypic analysis of transgenic plants showed that reduced growth of the *PtoIAA9m*-OE lines could be partially rescued by *PtoARF5.1*, whereas the truncated *PtoARF5.1* displayed stronger recovery than the full-length form (Fig. 4a). Quantitative measurement of plant height and stem diameter confirmed these changes in different transgenic lines (Fig. 4b,c). By contrast with the partial recovery (*c.* 50%) by the full-length *PtoARF5.1*, the *PtoARF5.1Δ* almost completely rescued the decreased stem diameter of the *PtoIAA9m-OE* plants relative to that of WT (Figs 4c, S7d). Stem cross-sectioning was conducted to establish if rescue of secondary xylem growth by constitutive expression of *PtoARF5.1* occurred in the *PtoIAA9m*-OE lines (Fig. 4d–f). Both the full-length and the truncated *PtoARF5.1* were able to rescue the inhibition of overexpressing *PtoIAA9m* on secondary xylem development, as evidenced by the increased number of xylem cell layers and xylem percentage (40% by *PtoARF5.1* and 94% by *PtoARF5.1Δ*) in stems (Fig. 4d–f). Noticeably, *PtoARF5.1Δ* conferred stronger recovery of the *PtoIAA9m*-OE-resulting defective wood formation than the full-length *PtoARF5.1* (Fig. 4d–f), leading to even more xylem cell layers than WT.

Subsequently, the cambium zone and its adjacent cell layers were characterized in detail to reveal the possible modulation of cell differentiation by the PtoIAA9–PtoARF5 module (Fig. 5). By contrast with the absence of EDX in *PtoIAA9m*-OE plants, these cell layers reoccurred in both *PtoARF5.1* and *PtoARF5.1Δ*-complementing lines (Fig. 5a). Similar recovery of defective xylem cell expansion resulting from overexpression of *PtoIAA9m* was detected for *PtoARF5.1* and *PtoARF5.1Δ*, as indicated by measurement of fiber and vessel cell size (Fig. 5b–d). Moreover, elevated vessel density was also rescued by introduction of *PtoARF5.1* and *PtoARF5.1Δ* into the *PtoIAA9m*-OE lines (Fig. 5b,e). The stronger recovery of *PtoARF5.1Δ* than its full-length form indicated that the PB1 domain mediating AUX/IAA-ARF protein interactions compromises the rescue of *PtoIAA9m*-resulting phenotypes of secondary xylem differentiation. Therefore, PtoARF5 is able to drive the PtoIAA9-dependent cellular behaviors for secondary xylem differentiation in poplar.

The PtoIAA9–PtoARF5 module directly regulates expression of *PtoHB7/8*

Diverse auxin-triggered developmental phenotypes depend on expression of specific batteries of auxin responsive genes targeted by Aux/IAA-ARF pairs (Vanneste & Friml, 2009). To identify auxin responsive genes targeted by the PtoIAA9–PtoARF5 module during wood formation in poplar, comparative transcriptomic profiling via RNAseq was performed with the *PtoIAA9m*-OE lines and WT, revealing 3873 differentially expressed genes (fold change ≥ 2 and false discovery rate $\leq 1\%$; Fig. S8a;

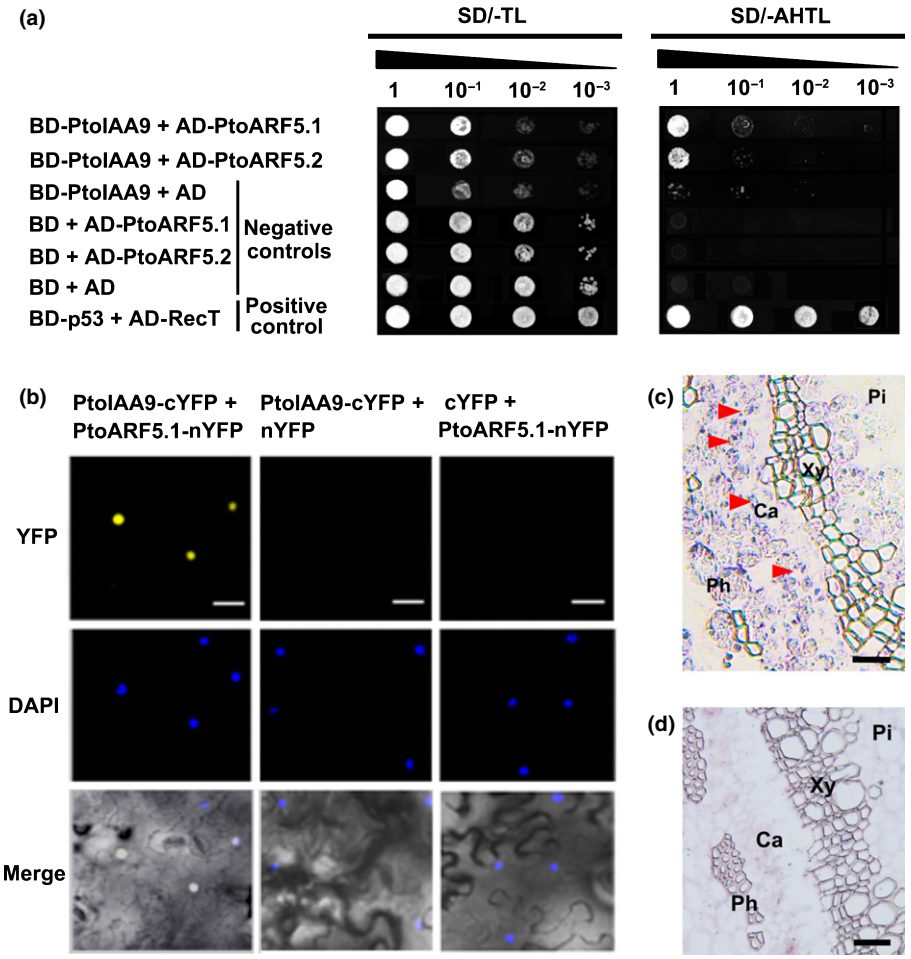

Fig. 3 Protein interactions of PtoIAA9 with PtoARF5s and expression of *PtoARF5* in secondary vascular tissues of *Populus tomentosa* stem. (a) Yeast-two-hybrid analysis of protein interactions between PtoIAA9 and PtoARF5.1/5.2. PtoIAA9 and PtoARF5.1/5.2 were fused with a Gal4 DNA-binding domain (BD) and a GAL4 activation domain (AD), respectively. The interaction between BD-p53 and AD-RecT (SV40 large T-antigen) was used as a positive control, while those between blank constructs (BD or AD) with BD-PtoIAA9 or AD-PtoARF5.1/5.2 were used as negative controls. Yeast cells were inoculated on selective medium in a 10-fold gradient dilution. SD/-TL, double dropout medium lacking tryptophan and leucine; SD/-AHTL, quadruple dropout medium lacking adenine, histidine, tryptophan and leucine. (b) Bimolecular fluorescence complementation (BiFC) assays validating physical interactions between PtoIAA9 and PtoARF5 in nuclei. nYFP and cYFP represent the N- and C-terminal part of yellow fluorescent protein (YFP), respectively. The PtoIAA9-nYFP and PtoARF5.1-cYFP constructs were cotransfected into tobacco epidermal leaf cells via *Agrobacterium*-mediated infiltration. The blank constructs of cYFP or nYFP were cotransfected with PtoIAA9-nYFP or PtoARF5.1-cYFP, respectively, as negative controls. The fluorescence emitted by YFP was examined with a confocal microscope. Nuclei were identified by DAPI staining. (c, d) RNA *in situ* hybridization of *PtoARF5* in secondary vascular tissues of poplar stem. The 7th internodes of 6-wk-old poplar plants cultivated in soil were cross-sectioned for hybridization with sense (c) and anti-sense (d) probes. The probes were designed within the identical region of *PtoARF5.1* and *PtoARF5.2* for detection of both *ARF5* paralogs in poplar. Red triangles indicate the *in situ* hybridization signals. Ca, cambium; Ph, phloem; Pi, pith; Xy, xylem. Bars: (b) 50 μm; (c, d) 200 μm.

Methods S1; Dataset S1). A number of *Aux/IAA*s, *SAUR*s and *GH3*s, which fall into classic families of early auxin responsive genes in plants (Guilfoyle, 1999), displayed significantly reduced transcript abundance (2.1- to 15.2-fold) in the *PtoIAA9m*-OE lines (Fig. S7b), suggesting that auxin signaling was weakened by *PtoIAA9m* overexpression in poplar. Gene ontology (GO) analysis of differentially expressed genes showed enrichment of the term of nucleic acid binding transcription factor activity (Fig. S7c). We thus investigated the differentially expressed genes encoding transcription factors that are known to regulate wood formation in poplar (Fig. S7d). All of these genes, including *WND*s, *ANT* and *HB*s, displayed decreased expression in the *PtoIAA9m*-OE lines (Fig. S8d). It has previously been established that class III HD-ZIP transcription factors are critical regulators of vascular formation and patterning in plants (Ramachandran *et al.*, 2017). This family, designated HB transcription factors, comprises eight members in poplar (Fig. S8e). RNAseq and qRT-PCR showed that five of them displayed *PtoIAA9m*-inhibited expression (Fig. S8d,f). Among them, PtoHB7 and PtoHB8 were identified as critical regulators of vascular cambium differentiation to secondary xylem in poplar (Zhu *et al.*, 2013). Therefore, we investigated whether the *PtoHB7/8* genes are downstream targets of PtoIAA9–PtoARF5 during wood formation.

To test this hypothesis, we determined the regulation of PtoIAA9–PtoARF5 on *PtoHB7* in the *PtoIAA9m*-OE lines. As

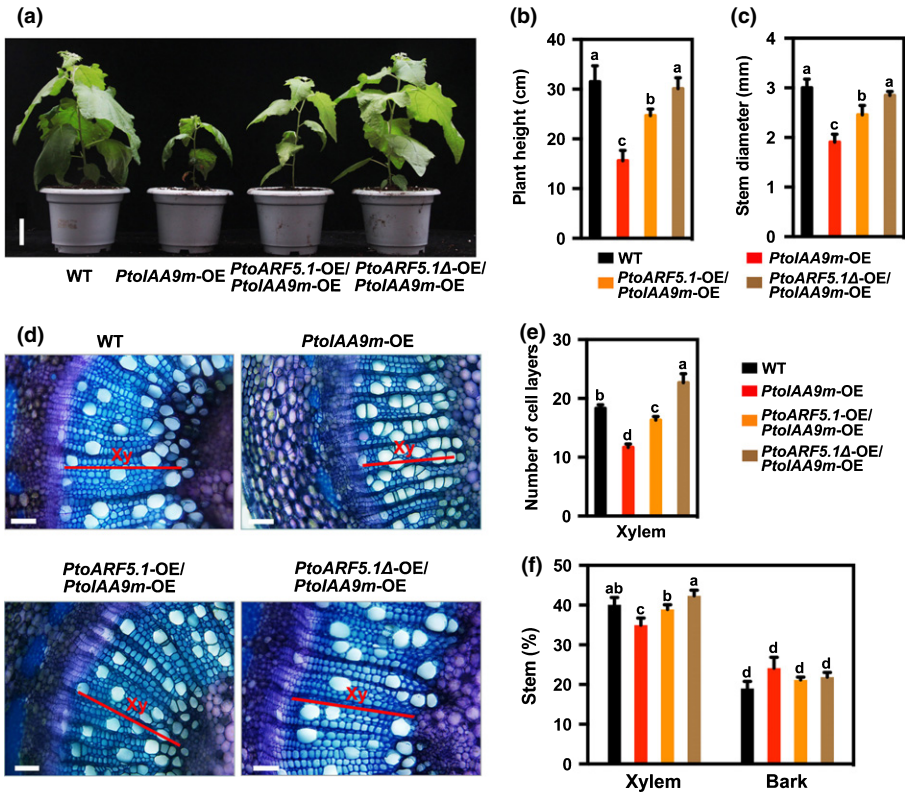

Fig. 4 Rescue of *PtoIAA9m*-resulting wood-associated phenotypes in *Populus tomentosa* by *PtoARF5*. (a) Recovered morphological phenotypes of 1.5-month-old *PtoIAA9m*-overexpressing (OE) transgenic poplar plants by *PtoARF5*. The constructs of *35S:PtoARF5.1* and *35S:PtoARF5.1Δ* (encoding for 1–665 amino acids of PtoARF5.1 without C-terminal III/IV domains) were transformed into poplar in the background of *PtoIAA9m*-OE. (b, c) Measurement of plant height and stem diameter of wild-type (WT), *PtoIAA9m*-OE, *PtoARF5.1*-OE/*PtoIAA9m*-OE and *PtoARF5.1Δ*-OE/*PtoIAA9m*-OE transgenic poplar lines. (d) Anatomical sections stained with toluidine blue of the 7th internode of 1.5-month-old WT, *PtoIAA9m*-OE, *PtoARF5.1*-OE/*PtoIAA9m*-OE and *PtoARF5.1Δ*-OE/*PtoIAA9m*-OE plants. Red lines indicate xylem. Xy, xylem. (e) Quantification of secondary xylem cell layers of WT, *PtoIAA9m*-OE, *PtoARF5.1*-OE/*PtoIAA9m*-OE and *PtoARF5.1Δ*-OE/*PtoIAA9m*-OE lines. The number of xylem cell layers was counted in toluidine blue-stained anatomical sections of the 7th internode of WT, *PtoIAA9m*-OE, *PtoARF5.1*-OE/*PtoIAA9m*-OE and *PtoARF5.1Δ*-OE/*PtoIAA9m*-OE plants. (f) Percentage of secondary xylem and bark in the stem of WT, *PtoIAA9m*-OE, *PtoARF5.1*-OE/*PtoIAA9m*-OE and *PtoARF5.1Δ*-OE/*PtoIAA9m*-OE plants. The area of secondary xylem, bark and total stem was quantified via ImageJ in toluidine blue-stained cross-sections of the 7th internode of WT, *PtoIAA9m*-OE, *PtoARF5.1*-OE/*PtoIAA9m*-OE and *PtoARF5.1Δ*-OE/*PtoIAA9m*-OE plants. Error bars represent SD. The letters above error bars indicate statistically significant differences (one-way ANOVA followed by Dunnett's test for pairwise comparisons; $n = 4$). Bars: (a) 5 cm; (d) 100 μm.

shown in Fig. 6(a), the expression of both *PtoHB*s was significantly decreased by 71% and 74% in the *PtoIAA9m*-OE lines, respectively, and could be rescued by the introduction of the truncated *PtoARF5.1* to even higher levels than that of WT. We also found that expression of *PtoHB7* and *PtoHB8* was increased 3.9- and 1.9-fold, respectively, in response to auxin treatment (Fig. 6b). Noticeably, overexpression of *PtoIAA9* almost completely blocked the auxin-induced expression of both *PtoHB7* and *PtoHB8* in the wood-forming stem (Fig. 6b), indicating that the auxin responsive expression of *PtoHB7* and *PtoHB8* is dependent on PtoIAA9. Promoter sequence analysis revealed that a series of core and canonical auxin response elements (*AuxRE*s), potential DNA binding sites for ARFs, are predicted in the 1.5 kb upstream regions of the start codons of *PtoHB7* and *PtoHB8* (Fig. 6c,d). ChIP was performed using *PtoARF5.1-HA* transgenic plants and the enrichment of *AuxRE*s harbored by the *PtoHB7* and *PtoHB8* promoters was quantified by qPCR (Fig. 6e,f). In comparison with negative controls, some *AuxRE*-containing promoter regions of *PtoHB7* (Regions II/III) and *PtoHB8* (Regions III/IV) were significantly enriched after immunoprecipitation (Fig. 6e,f), indicating the direct binding of PtoARF5.1 to their promoters. The PtoIAA9/PtoARF5-dependent regulation of *PtoHB7/8* was subsequently confirmed by effector–reporter assays in transiently expressed tobacco leaves. The reporter constructs carrying the *GUS* reporter gene driven by the 1.5 kb promoter regions of *PtoHB7* and *PtoHB8*, respectively, were co-transfected with different combinations of the effectors harboring PtoIAA9 and PtoARF5.1 (Fig. S9). Determination of GUS activity revealed that PtoARF5.1 was able to independently activate expression of *PtoHB7*, whereas the activation was completely abolished by the addition of PtoIAA9 ($P < 0.05$; Fig. S9a). By contrast, PtoIAA9 did not compromise the activation induced by PtoARF5.1Δ without the C-terminal III/IV domains, indicating that PtoIAA9-mediated repression of *PtoHB7* expression relies on its interactions with PtoARF5.1 via the III/V domains. Similar results were obtained from the promoter of *PtoHB8* (Fig. S9b).

To further validate direct regulation of PtoARF5.1 on *PtoHB*s via binding to *AuxRE*s, short promoter fragments harboring

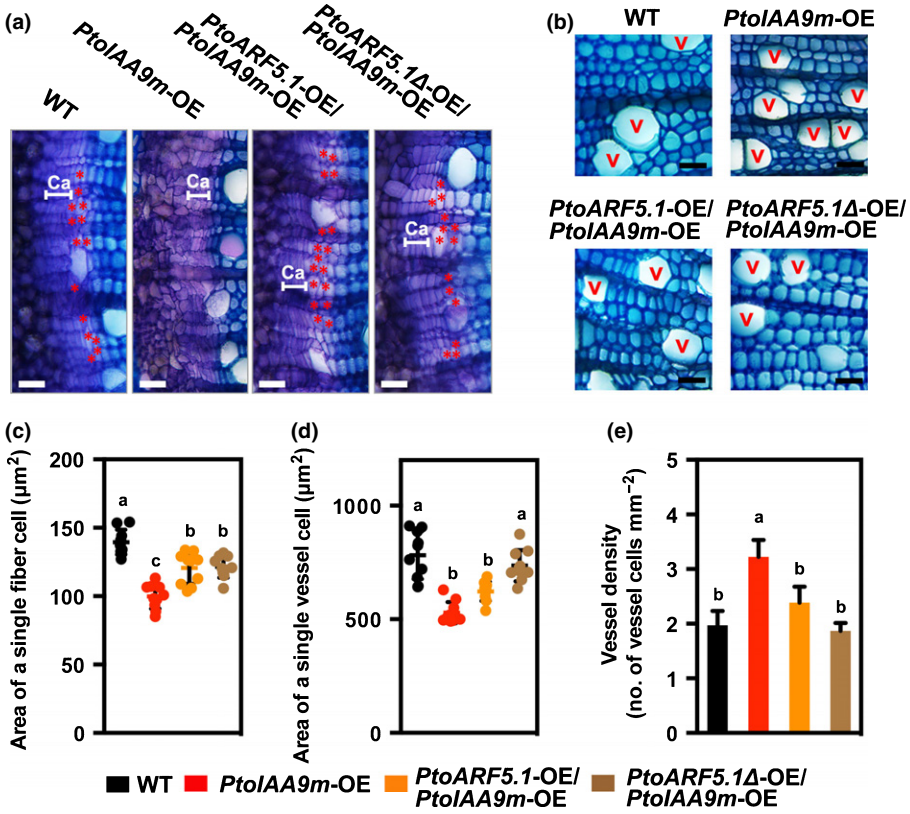

Fig. 5 *PtoARF5* restores *PtoIAA9*-affected phenotypes of secondary xylem cells in *Populus tomentosa* during wood formation. (a, b) Detailed observation of cambial zone and woody cells of secondary xylem in wild-type (WT), *PtoIAA9m*-OE, *PtoARF5.1*-OE/*PtoIAA9m*-OE and *PtoARF5.1Δ*-OE/*PtoIAA9m*-OE plants. The images were captured on toluidine blue-stained anatomical sections of the 7th internode of the corresponding lines. White lines indicate cambium (Ca), and red stars represent the cells of early developing xylem (EDX). V, vessel. Bars, 50 μm. (c, d) Quantification of size of a single fiber and vessel cell in stems of WT, *PtoIAA9m*-OE, *PtoARF5.1*-OE/*PtoIAA9m*-OE and *PtoARF5.1Δ*-OE/*PtoIAA9m*-OE plants. The area of fiber and vessel cells was measured and calculated via ImageJ based on images of toluidine blue-stained anatomical sections as described in the Materials and Methods. (e) Density of vessels in stems of WT, *PtoIAA9m*-OE, *PtoARF5.1*-OE/*PtoIAA9m*-OE and *PtoARF5.1Δ*-OE/*PtoIAA9m*-OE plants. The number of xylem vessels was counted based on images of toluidine blue-stained anatomical sections. Error bars represent SD. The letters above error bars indicate significant differences (one-way ANOVA followed by Dunnett's test for pairwise comparisons; $n = 10–12$).

canonical *AuxRE*s (−447 to −581 bp upstream of the start codon of *PtoHB7*, and −344 to −434 bp upstream of the start codon of *PtoHB8*), which were strongly enriched in ChIP assays, were constructed to drive the firefly luciferase reporter. Consistently, PtoARF5.1 significantly activated the expression of luciferase reporter driven by the *AuxRE*-harbored promoter fragments of *PtoHB7*/*8* ($P < 0.05$; Fig. 6g). By contrast, *PtoARF5.1*-driven activation disappeared when the *AuxRE*s harbored in the promoter fragments of *PtoHB7* and *PtoHB8* were disrupted by site-directed mutagenesis (Fig. 6g). Therefore, the PtoIAA9–PtoARF5 module directly regulates the expression of *PtoHB7* and *PtoHB8* via binding of PtoARF5 to the *AuxRE*s within their promoters.

PtoHB7 partially rescues *PtoIAA9m*-resulting phenotypes of wood formation

To establish the link of biological functions between auxin signaling and the HB transcription factors during wood formation, we conducted complementation of the *PtoIAA9m*-resulting impaired secondary xylem phenotypes by *PtoHB7* via stable transformation (Figs 7, S9). Phenotypic characterization revealed partial recovery of the *PtoIAA9m*-repressing plant growth and stem development by *PtoHB7* (Fig. S10b–d). Stem cross-sections showed that introduction of *PtoHB7* into the *PtoIAA9m*-OE background could partially rescue the impaired secondary xylem development, as validated by the quantification of xylem cell layers (Fig. 7a,b). Constitutive expression of *PtoHB7* led to the reoccurrence of the EDX cell layers, which were repressed in the *PtoIAA9m*-OE lines (Fig. 7c). Similarly, the decreased cell size of xylem fibers and vessels as well as the enhanced vessel density were partially rescued by the introduction of *PtoHB7* into the *PtoIAA9m*-OE plants (Fig. 7d–h).

Moreover, we determined the expression of several genes, including *ACL5*, *CesA7A*, *PAL4*, *GT43B* and *WND1B*, which were previously reported *HB7*/*8*-regulated genes involved in wood formation of poplar (Milhinhos *et al.*, 2013; Zhu *et al.*, 2013). The down-regulated expression of these genes in *PtoIAA9m*-OE plants was at least partially rescued in *PtoARF5.1*- and *PtoHB7*-complementing transgenic lines (Fig. S11). A similar result was obtained in *EXPA1*, a marker gene for cell expansion during wood formation (Sundell *et al.*, 2017). We also

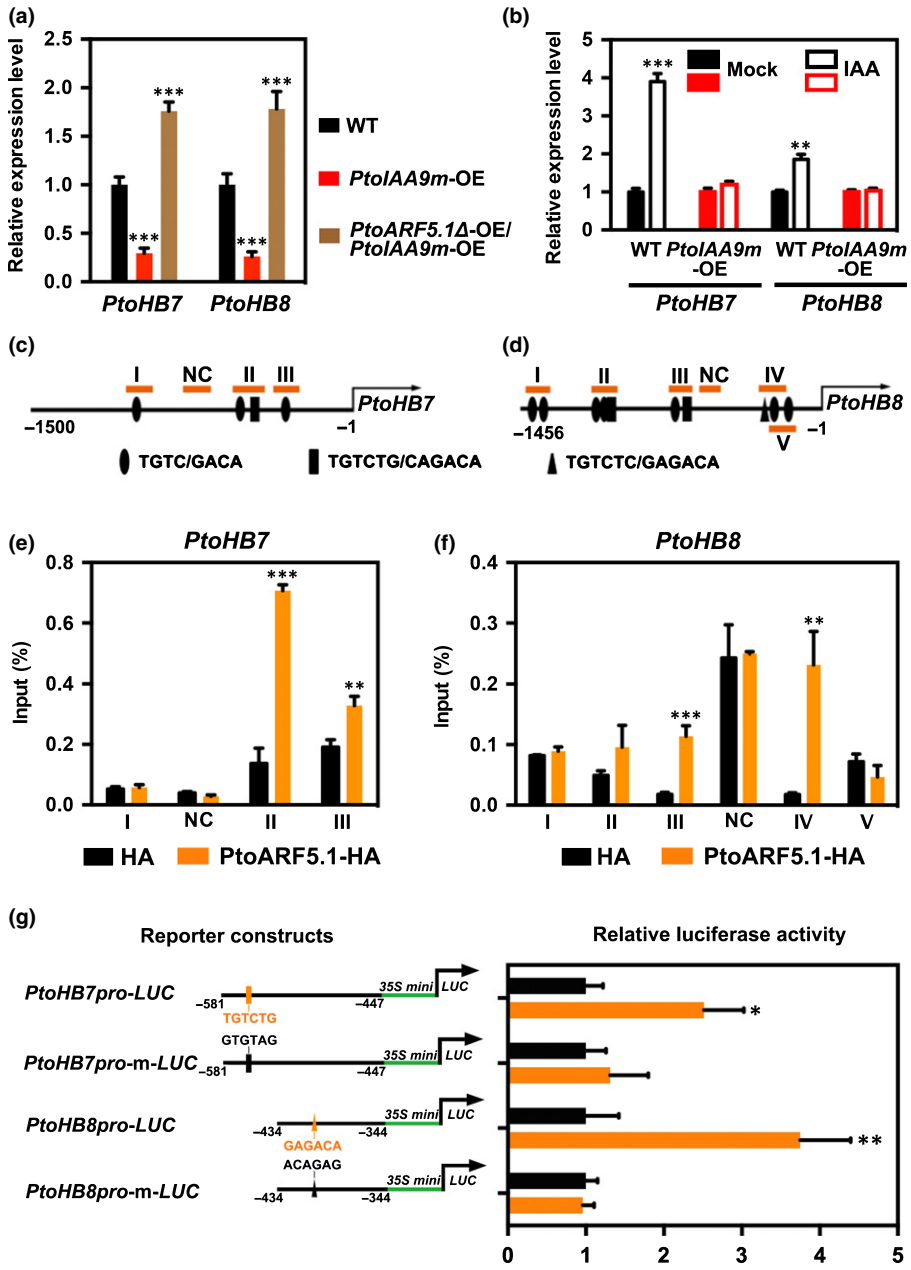

Fig. 6 Direct regulation of PtoIAA9/ARF5 on *PtoHB7* and *PtoHB8* in *Populus tomentosa*. (a) Expression levels of *PtoHB7* and *PtoHB8* in wild-type (WT), *PtoIAA9m*-OE and *PtoARF5.1Δ*-OE/*PtoIAA9m*-OE lines determined by qRT-PCR. Stem tissues of 6-wk-old poplar plants cultivated in soil were collected for RNA extraction. 18S rRNA was used as a reference gene. WT values were normalized to 1. (b) Auxin-induced expression of *PtoHB7* and *PtoHB8* in WT and *PtoIAA9m*-OE lines. Microcutting-propagated poplar seedlings cultivated *in vitro* for 4 wk were subjected to 5 μM IAA for 6 h, and stem tissues were collected for RNA extraction followed by qRT-PCR assays. 18S rRNA was used as a reference gene. The values for mock treatment were normalized to 1. For (a, b), error bars represent SD, and one-way ANOVA followed by Dunnett's test for pairwise comparisons with respect to values of WT (a) or mock treatment (b) was performed to detect statistically significant differences (**, $P < 0.001$; ***, $P < 0.001$; $n = 4$). (c, d) Distribution of canonical and core auxin response elements (*AuxREs*) harbored in the promoter regions of *PtoHB7* (c) and *PtoHB8* (d). Orange lines with I–III indicate *AuxRE*-harbored fragments amplified by ChIP-qPCR, while NC represents *AuxRE*-free negative control. (e, f) ChIP-qPCR analysis of PtoARF5 protein fused with HA tag with the promoter region of *PtoHB7* (e) and *PtoHB8* (f). Shoot tissues of 1-month-old poplar plants were used. Error bars represent SD. Student's *t*-test was performed to evaluate significant differences between values of WT and those of PtoARF5.1-HA for each region (**, $P < 0.01$; ***, $P < 0.001$; $n = 3$). (g) *AuxRE*-dependent transactivation via transient cotransformation assay. For reporters, the 1-kb promoter fragments of *PtoHB7* and *PtoHB8* were constructed to drive the expression of firefly luciferase (LUC). The *AuxREs* found in these promoter fragments were disrupted via site-directed mutagenesis to generate *PtoHB7/8pro*-m-LUC. The effector encodes PtoARF5.1 driven by the *CaMV 35S* promoter. Ratios of firefly luciferase to *Renilla* luciferase activity after cotransformation into tobacco leaf epidermal cells with different reporter and effector construct combinations were tested. Values for the blank effector were normalized to 1. Error bars represent SD. Student's *t*-test was performed to evaluate significant differences between values of blank effector and those of PtoARF5.1 (*, $P < 0.05$; **, $P < 0.01$; $n = 3$).

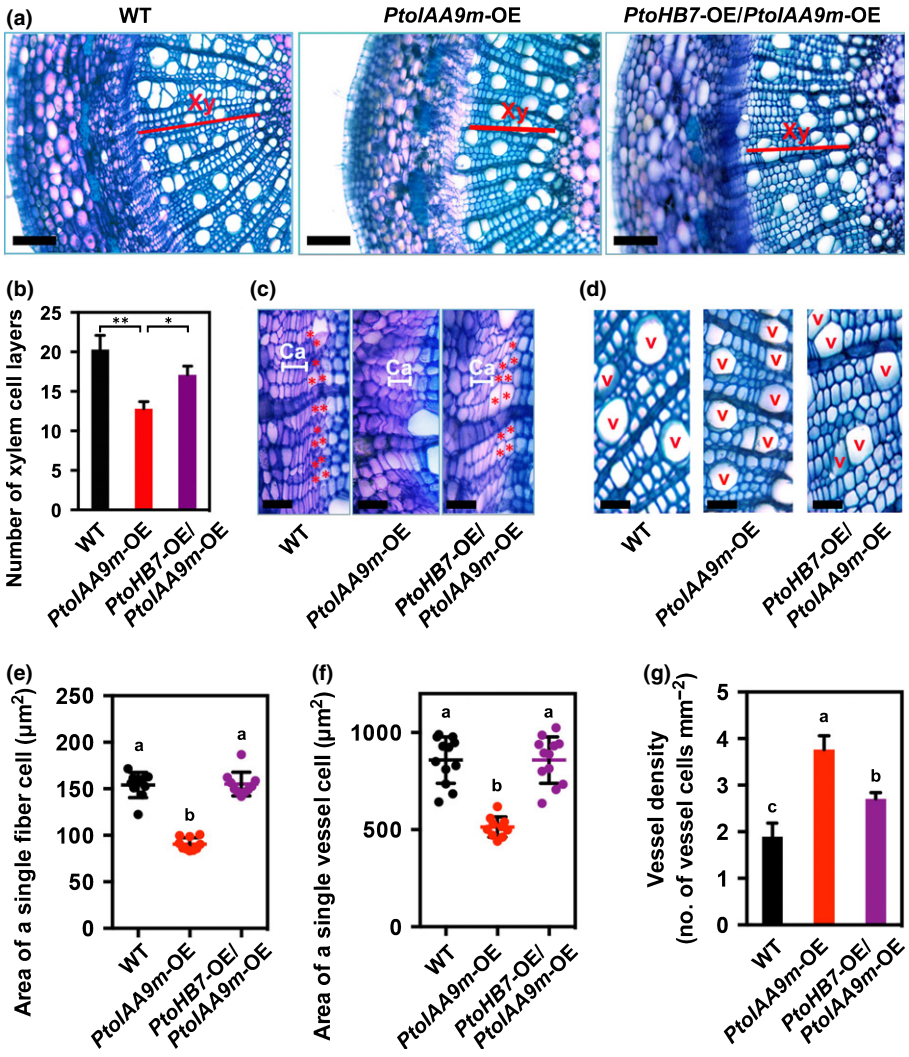

Fig. 7 *PtoHB7* partially rescues deficient phenotypes of wood formation resulting from constitutive expression of *PtoIAA9* in *Populus tomentosa*. (a) Cross-sections stained with toluidine blue of the 7th internode of 1-month-old WT, *PtoIAA9m*-OE and *PtoHB7*-OE/*PtoIAA9m*-OE lines. Red lines indicate xylem. Xy, xylem. (b) Number of xylem cell layers of wild-type (WT), *PtoIAA9m*-OE and *PtoHB7*-OE/*PtoIAA9m*-OE lines. (c, d) Detailed phenotypes of cambial zone and woody cells of secondary xylem in wood-forming stem of WT, *PtoIAA9m*-OE and *PtoHB7*/*PtoIAA9m*-OE plants. The images were captured on toluidine blue-stained anatomical sections of the 7th internode of the corresponding lines. White lines indicate cambium (Ca), and red stars represent the cells of early developing xylem (EDX). V, vessel. (e, f) Quantification of size of a single fiber and vessel cell in stems of WT, *PtoIAA9m*-OE, and *PtoHB7*/*PtoIAA9m*-OE plants. The area of fiber and vessel cells was measured and calculated via ImageJ based on images of toluidine blue-stained anatomical sections as described in the Materials and Methods. (g) Density of vessels in stem of WT, *PtoIAA9m*-OE and *PtoHB7*/*PtoIAA9m*-OE plants. The number of xylem vessels was counted based on the images of toluidine blue-stained anatomical sections. Error bars represent SD. The letters above error bars indicate significant differences (one-way ANOVA followed by Dunnett's test for pairwise comparisons; $n = 10–12$). Bars: (a) 100 μm; (c, d) 50 μm.

found that expression of *WND6A* and *B*, which are the closest homologs of Arabidopsis *VND6* and *VND7* (Zhong *et al.*, 2011), was enhanced by *PtoIAA9m* overexpression, but was rescued by *PtoARF5.1* and *PtoHB7* (Fig. S11), in accordance with elevated vessel formation by *PtoIAA9m*-OE and complemented by *PtoARF5* and *PtoHB7*. These results strongly suggest that auxin-induced secondary xylem development depends on the activation of the *PtoHB* genes by the PtoIAA9/PtoARF5 complex in poplar.

Discussion

Auxin is considered a positional signal that drives cambium-derived wood formation (Uggla *et al.*, 1996). Previous studies have demonstrated auxin-mediated regulation of cambial cell division in trees (Sundberg *et al.*, 2000; Nilsson *et al.*, 2008). However, a highly sensitive analysis of auxin signaling in Arabidopsis revealed its maximal levels in differentiating cambial descendants, spatially divergent from the maximum auxin concentration in cambial initials (Brackmann *et al.*, 2018). In this study, we report that auxin coordinates multiple aspects of the cellular changes occurring for cambium specification into secondary xylem through the IAA9-ARF5 pathway in *Populus*. We further demonstrate that the PtoIAA9–PtoARF5 module directly targets *PtoHB7* and *PtoHB8* to mediate auxin-triggered early developing xylem (EDX) cell differentiation during wood formation.

Aux/IAA proteins function as molecular switches of auxin signaling conserved among flowering plants (Paponov *et al.*, 2009). Comprehensive analyses of *Populus Aux/IAA*s revealed variable levels and spatial patterns of expression across wood-forming tissues (Fig. S2), implying functional diversification in wood formation (Moyle *et al.*, 2002; Kalluri *et al.*, 2007). The transcripts of *IAA9*, *-16.1* and *-16.2* were enriched in cambium-neighboring cells undergoing differentiation into xylem but declined with xylem maturation (Fig. S2c). Highly correlated expression patterns among these *Aux/IAA* genes (Fig. S2c,d) and common protein interactions with ARF5 (Fig. S6d) suggested their functional redundancy in wood formation. Although compromised, wood differentiation could not be completely suspended by overexpressing *PtoIAA9*, implying regulatory complexity depending on some other pathways besides auxin signaling.

Compromised auxin signaling by expressing stable Aux/IAAs allows auxin-mediated coordination of cellular behaviors during wood formation to be explored. Overexpression of a hybrid aspen *IAA3* (*PttIAA3*) attenuates periclinal cell division in cambium but enlarges cell files harboring anticlinal cell division, suggesting dual regulation of auxin signaling on cambial proliferation (Nilsson *et al.*, 2008). Despite more tightly arranged cambial cells (Fig. 2g), however, overexpressing *PtoIAA9* did not lead to significant changes in cambial cell layers (Fig. S5e), implicating its weak role in cambial activity. *IAA20.1* and *-20.2*, the *PttIAA3* homologs in our nomenclature, displayed much lower expression levels than *IAA9*, and different expression patterns from *IAA9* during wood formation (Fig. S2). Aux/IAAs usually require functional cooperation of ARFs via protein interactions, and harbor variable interacting affinities with different ARFs (Vanneste & Friml, 2009). Thus, specific ARF partners of PttIAA3 and PtoIAA9 may cause their differential regulation on cambial activity.

Compared to WT, the proportion of woody tissues of transgenic plants overexpressing *PtoIAA9m* was significantly reduced (Fig. 2e, f), implying inhibition of secondary xylem development by *PtoIAA9*. Both reduced xylem cell layers and restricted xylem cell size led to *PtoIAA9*-inhibited wood formation that was rescued by overexpressing *PtoARF5* (Figs 2, 4, 5). Cambial proliferation and cambium specification to xylem cooperatively determine the number of xylem cell layers (Sanchez *et al.*, 2012). Given the excluded *PtoIAA9*-mediated effects on cambial proliferation, we propose that the reduced periclinal cell division rate may be responsible for *PtoIAA9*-repressed wood formation. This is supported by the disappearance and reappearance of the EDX cell layers in *PtoIAA9*-overexpressing and *PtoARF5.1*-complementing lines, respectively (Figs 2, 5). These cell layers are initially specified from cambial cells and at early stage of wood formation. Active cambium periclinal cell division leads to rapid xylem mother cell accumulation, while a low rate of cambium periclinal cell division slowly produces xylem mother cells, resulting in an absence of the EDX cell layers in the *PtoIAA9m*-OE lines. Similar phenotypes were also found in trees during dormancy (Gričar *et al.*, 2014). Therefore, specification and expansion of xylem cells during wood differentiation are coordinated by IAA9-ARF5-mediated auxin signaling in poplar.

Recent studies have shown that Arabidopsis MP/ARF5 directly represses *WOX4* expression for restrained stem cell quantity

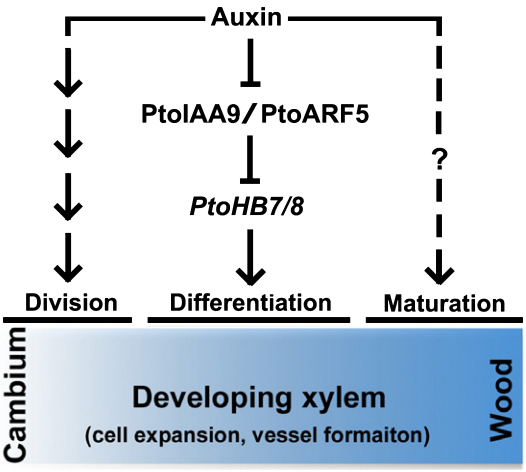

Fig 8 A model for Aux/IAA-ARF-HB-dependent wood formation in *Populus tomentosa*. Auxin displays complex regulation of various steps during wood formation in poplar. The auxin-dependent cambial cell division was demonstrated by Nilsson *et al.* (2008). The role of auxin in xylem maturation, mainly including secondary wall deposition, remained unclear. In this study, PtoIAA9-ARF5-HB7/8-mediated wood differentiation is proposed. The auxin-dependent PtoIAA9-ARF5 module directly regulates the expression of *PtoHB7/8*, which drives multiple cellular events including xylem cell specification, expansion and vessel formation during secondary xylem development. Arrows represent a positive regulatory action of one component on another. Lines ending with a trait represent a negative regulatory action. Dotted lines indicate indirect regulation.

(Brackmann *et al.*, 2018), and switches of MP/ARF5 phosphorylation mediated by BIL1 kinase integrate peptide and cytokinin signaling for cambial activity (Han *et al.*, 2018). Here we provide evidence in *Populus* that ARF5 coordinates multiple behaviors for woody cell differentiation via directly targeting HB7/8 paralogs. BDL/IAA12 is a canonical Aux/IAA partner of ARF5/MP in Arabidopsis during embryogenesis (Hamann *et al.*, 2002). Due to promiscuous protein interactions between Aux/IAAs and ARFs, cooperative functions of IAA12-ARF5 could not be excluded in poplar. The significantly lower transcript abundance of *IAA12* paralogs than *IAA9* and their different expression patterns in wood-forming stems (Fig. S2) suggest possible variable roles in wood differentiation. We expected that IAA9 also regulates procambial specification during root development and leaf vein pattering. Indeed, the knockdown of *IAA9* in tomato led to abnormal leaf formation with different vascular tissue patterning (Wang *et al.*, 2005).

Arabidopsis HD-ZIP III transcription factors are key regulators in orchestrating vascular patterning in developmental contexts of root, leaf and stem (Ramachandran *et al.*, 2017). *AtHB8* displays specific expression in procambial cells and is involved in vascular differentiation (Baima *et al.*, 2001). *HB7*, the poplar ortholog of *AtHB8*, has been revealed to be a dose-dependent regulator that balances cambium activity and xylem differentiation during secondary growth (Zhu *et al.*, 2013). We found that a series of core and canonical auxin response elements (*AuxREs*), the potential DNA binding sites for ARFs, are present in the promoters of poplar *HB7* and *HB8*. ChIP and effector–reporter tests revealed transcriptional activation of *PtoARF5.1* via

direct binding to the *AuxRE* elements harbored in the promoters of *HB* genes (Fig. 6). Importantly, PtoHB7 is able to functionally rescue phenotypes of xylem cell specification, expansion and vessel density (Fig. 7). Therefore, our data suggested that the PtoIAA9–PtoARF5 module directly targets *PtoHB7* and *PtoHB8* for regulating secondary cell differentiation. In Arabidopsis, ARF5/MP has been identified to control leaf vein patterning by directly targeting *AtHB8* (Donner *et al.*, 2009), demonstrating ARF5-HB7/8 as a conserved pathway for vascular patterning of leaves and stems in herbaceous and woody species. Moreover, the *HB8* orthologs can directly regulate the expression of *ACL5* encoding thermospermine synthase in both Arabidopsis and poplar for xylem differentiation, and also form a feedback regulation on the auxin pathway (Milhinhos *et al.*, 2013; Baima *et al.*, 2014). We also found that the expression of *ACL5* was significantly decreased by *PtoIAA9* overexpression and rescued by *PtoARF5* complementation (Fig. S11).

Collectively, our data allow us to propose a model for IAA9-ARF5-mediated coordination for wood differentiation (Fig. 8). Auxin releases the repression of PtoIAA9, by triggering its protein degradation, on PtoARF5-activated auxin responsive gene expression during cambium-derived wood formation. In parallel, auxin-inducible transcript abundance of *PtoIAA9* switches-off auxin signaling in a self-controlled manner. The PtoIAA9–PtoARF5 module directly targets *PtoHB7* and *PtoHB8* to mediate auxin regulation on multiple cellular events, including xylem specification, expansion and vessel formation for secondary xylem development. In conclusion, our findings show that the auxin-Aux/IAA-ARF pathway plays a key role in controlling wood formation via HB-driven cambium differentiation in *Populus*.

Acknowledgements

We thank Drs Guoqing Niu, Xinqiang He and Jianquan Liu for helpful comments. This work was supported by the National Natural Science Foundation of China (31500544, 31670669, 31870657, 31800505 and 31870175), National Key Project for Research on Transgenic Plant (2016ZX08010-003) and Fundamental Research Funds for the Central Universities (XDJK2018AA005, XDJK2014a005). The authors declare no conflicts of interest.

Author contributions

KL, CX and HCW designed the work; CX, FH, YS, XF, WL, CL, HY, YL and DF performed experiments and data analyses; CX drafted the manuscript; KL and HCW revised the manuscript. All authors approved the final version of the manuscript for publication. CX, YS, FH, XF and HY contributed equally to this work.

ORCID

Keming Luo https://orcid.org/0000-0003-4928-7578

References

Baima S, Forte V, Possenti M, Penalosa A, Leoni G, Salvi S, Felici B, Ruberti I, Morelli G. 2014. Negative feedback regulation of auxin signaling by ATHB8/ACL5-BUD2 transcription module. *Molecular Plant* **7**: 1006–1025.

Baima S, Possenti M, Matteucci A, Wisman E, Altamura MM, Ruberti I. 2001. The Arabidopsis ATHB-8 HD-zip protein acts as a differentiation-promoting transcription factor of the vascular meristems. *Plant Physiology* **126**: 643–655.

Bargmann BO, Vanneste S, Krouk G, Nawy T, Efroni I, Shani E, Choe G, Friml J, Bergmann DC, Estelle M *et al.* 2013. A map of cell type-specific auxin responses. *Molecular Systems Biology* **9**: 688.

Björklund S, Antti H, Uddestrand I, Moritz T, Sundberg B. 2007. Cross-talk between gibberellin and auxin in development of *Populus* wood: gibberellin stimulates polar auxin transport and has a common transcriptome with auxin. *The Plant Journal* **52**: 499–511.

Bonan GB. 2008. Forests and climate change: forcings, feedbacks, and the climate benefits of forests. *Science* **320**: 1444–1449.

Brackmann K, Qi J, Gebert M, Jouannet V, Schlamp T, Grünwald K, Wallner ES, Novikova DD, Levitsky VG, Agustí J *et al.* 2018. Spatial specificity of auxin responses coordinates wood formation. *Nature Communications* **9**: 875.

Campbell L, Turner S. 2017. Regulation of vascular cell division. *Journal of Experimental Botany* **68**: 27–43.

Chen S, Songkumarn P, Liu J, Wang G. 2009. A versatile zero background T-vector system for gene cloning and functional genomics. *Plant Physiology* **150**: 1111–1121.

Dejardin A, Laurans F, Arnaud D, Breton C, Pilate G, Leple JC. 2010. Wood formation in Angiosperms. *Comptes Rendus Biologies* **333**: 325–334.

Donner TJ, Sherr I, Scarpella E. 2009. Regulation of preprocambial cell state acquisition by auxin signaling in Arabidopsis leaves. *Development* **136**: 3235–3246.

Fukuda H. 2004. Signals that control plant vascular cell differentiation. *Nature Reviews Molecular Cell Biology* **5**: 379–391.

Gričar J, Prislan P, Gryc V, Vavrčík H, de Luis M, Čufar K. 2014. Plastic and locally adapted phenology in cambial seasonality and production of xylem and phloem cells in *Picea abies* from temperate environments. *Tree Physiology* **34**: 869–881.

Guilfoyle TJ. 1999. Auxin-regulated genes and promoters. In: Hooykaas PJJ, Hall M, Libbenga KL, eds. *Biochemistry and molecular biology of plant hormones.* Leiden, the Netherlands: Elsevier, 423–459.

Hamann T, Benkova E, Baurle I, Kientz M, Jurgens G. 2002. The Arabidopsis *BODENLOS* gene encodes an auxin response protein inhibiting MONOPTEROS-mediated embryo patterning. *Genes & Development* **16**: 1610–1615.

Han S, Cho H, Noh J, Qi J, Jung HJ, Nam H, Lee S, Hwang D, Greb T, Hwang I *et al.* 2018. BIL1-mediated MP phosphorylation integrates PXY and cytokinin signalling in secondary growth. *Nature Plants* **4**: 605–614.

Hardtke CS, Berleth T. 1998. The Arabidopsis gene *MONOPTEROS* encodes a transcription factor mediating embryo axis formation and vascular development. *EMBO Journal* **17**: 1405–1411.

Immanen J, Nieminen K, Smolander OP, Kojima M, Alonso Serra J, Koskinen P, Zhang J, Elo A, Mähönen AP, Street N *et al.* 2016. Cytokinin and auxin display distinct but interconnected distribution and signaling profiles to stimulate cambial activity. *Current Biology* **26**: 1990–1997.

Jefferson RA. 1987. Assaying chimeric genes in plants: the GUS gene fusion system. *Plant Molecular Biology Reporter* **5**: 387–405.

Jia Z, Sun Y, Yuan L, Tian Q, Luo K. 2010. The chitinase gene (*Bbchit1*) from *Beauveria bassiana* enhances resistance to *Cytospora chrysosperma* in *Populus tomentosa* Carr. *Biotechnology Letters* **32**: 1325–1332.

Johnson LA, Douglas CJ. 2007. *Populus trichocarpa MONOPTEROS/AUXIN RESPONSE FACTOR5* (*ARF5*) genes: comparative structure, subfunctionalization, and *Populus Arabidopsis* microsynteny. *Canadian Journal of Botany-Revue Canadienne De Botanique* **85**: 1058–1070.

Kalluri UC, Difazio SP, Brunner AM, Tuskan GA. 2007. Genome-wide analysis of *Aux/IAA* and *ARF* gene families in *Populus trichocarpa. BMC Plant Biology* **7**: 59.

Leyser O. 2005. Auxin distribution and plant pattern formation: how many angels can dance on the point of PIN? *Cell* **121**: 819–822.

Matte Risopatron J, Sun Y, Jones B. 2010. The vascular cambium: molecular control of cellular structure. *Protoplasma* **247**: 145–161.

Milhinhos A, Prestele J, Bollhoner B, Matos A, Vera-Sirera F, Rambla JL, Ljung K, Carbonell J, Blázquez MA, Tuominen H *et al.* 2013. Thermospermine levels are controlled by an auxin-dependent feedback loop mechanism in *Populus* xylem. *The Plant Journal* **75**: 685–698.

Mockaitis K, Estelle M. 2008. Auxin receptors and plant development: a new signaling paradigm. *Annual Review of Cell and Developmental Biology* **24**: 55–80.

Moyle R, Schrader J, Stenberg A, Olsson O, Saxena S, Sandberg G, Bhalerao RP. 2002. Environmental and auxin regulation of wood formation involves members of the *Aux/IAA* gene family in hybrid aspen. *The Plant Journal* **31**: 675–685.

Muller CJ, Valdes AE, Wang G, Ramachandran P, Beste L, Uddenberg D, Carlsbecker A. 2016. PHABULOSA mediates an auxin signaling loop to regulate vascular patterning in Arabidopsis. *Plant Physiology* **170**: 956–970.

Nakajima K, Benfey P. 2002. Signaling in and out: control of cell division and differentiation in the shoot and root. *Plant Cell* **14**(Suppl): S265–S276.

Nilsson J, Karlberg A, Antti H, Lopez-Vernaza M, Mellerowicz E, Perrot-Rechenmann C, Sandberg G, Bhalerao RP. 2008. Dissecting the molecular basis of the regulation of wood formation by auxin in hybrid aspen. *Plant Cell* **20**: 843–855.

Paponov IA, Teale W, Lang D, Paponov M, Reski R, Rensing SA, Palme K. 2009. The evolution of nuclear auxin signalling. *BMC Evolutionary Biology* **9**: 126.

Perrot-Rechenmann C. 2010. Cellular responses to auxin: division versus expansion. *Cold Spring Harbor Perspectives in Biology* **2**: a001446.

Przemeck GK, Mattsson J, Hardtke CS, Sung ZR, Berleth T. 1996. Studies on the role of the Arabidopsis gene *MONOPTEROS* in vascular development and plant cell axialization. *Planta* **200**: 229–237.

Ragauskas AJ, Williams CK, Davison BH, Britovsek G, Cairney J, Eckert CA, Frederick WJ Jr, Hallett JP, Leak DJ, Liotta CL *et al.* 2006. The path forward for biofuels and biomaterials. *Science* **311**: 484–489.

Ramachandran P, Carlsbecker A, Etchells J. 2017. Class III HD-ZIPs govern vascular cell fate: an HD view on patterning and differentiation. *Journal of Experimental Botany* **68**: 55–69.

Reed JW. 2001. Roles and activities of Aux/IAA proteins in Arabidopsis. *Trends in Plant Science* **6**: 420–425.

Sanchez P, Nehlin L, Greb T. 2012. From thin to thick: major transitions during stem development. *Trends in Plant Science* **17**: 113–121.

Sang XC, Li YF, Luo ZK, Ren D, Fang L, Wang N, Zhao F, Ling Y, Yang Z, Liu Y *et al.* 2012. CHIMERIC FLORAL ORGANS1, encoding a monocot-specific MADS box protein, regulates floral organ identity in rice. *Plant Physiology* **160**: 788–807.

Savidge RA. 1983. The role of plant hormones in higher plant cellular differentiation. II. Experiments with the vascular cambium, and sclereid and tracheid differentiation in the pine, *Pinus contorta*. *The Histochemical Journal* **15**: 447–466.

Sundberg B, Uggla C, Tuominen H. 2000. Cambial growth and auxin gradients. In: Savidge R, Barnett J, Napier R, eds. *Cell and molecular biology of wood formation*. Oxford, UK: BIOS Scientific Publishers, 169–188.

Sundell D, Street NR, Kumar M, Mellerowicz EJ, Kucukoglu M, Johnsson C, Kumar V, Mannapperuma C, Delhomme N, Nilsson O *et al.* 2017. AspWood: high-spatial-resolution transcriptome profiles reveal uncharacterized modularity of wood formation in *Populus tremula*. *Plant Cell* **29**: 1585–1604.

Tuominen H, Puech L, Fink S, Sundberg B. 1997. A radial concentration gradient of indole-3-acetic acid is related to secondary xylem development in hybrid aspen. *Plant Physiology* **115**: 577–585.

Turner S, Gallois P, Brown D. 2007. Tracheary element differentiation. *Annual Review of Plant Biology* **58**: 407–433.

Uggla C, Mellerowicz EJ, Sundberg B. 1998. Indole-3-acetic acid controls cambial growth in scots pine by positional signaling. *Plant Physiology* **117**: 113–121.

Uggla C, Moritz T, Sandberg G, Sundberg B. 1996. Auxin as a positional signal in pattern formation in plants. *Proceedings of the National Academy of Sciences, USA* **93**: 9282–9286.

Vanneste S, Friml J. 2009. Auxin: a trigger for change in plant development. *Cell* **136**: 1005–1016.

Wang H, Jones B, Li Z, Frasse P, Delalande C, Regad F, Chaabouni S, Latche A, Pech JC, Bouzayen M. 2005. The tomato Aux/IAA transcription factor IAA9 is involved in fruit development and leaf morphogenesis. *Plant Cell* **17**: 2676–2692.

Worley CK, Zenser N, Ramos J, Rouse D, Leyser O, Theologis A, Callis J. 2000. Degradation of Aux/IAA proteins is essential for normal auxin signalling. *The Plant Journal* **21**: 553–562.

Yang H, Han Z, Cao Y, Fan D, Li H, Mo H, Feng Y, Liu L, Wang Z, Yue Y *et al.* 2012. A companion cell-dominant and developmentally regulated H3K4 demethylase controls flowering time in Arabidopsis via the repression of *FLC* expression. *PLoS Genetics* **8**: e1002664.

Ye ZH, Zhong R. 2015. Molecular control of wood formation in trees. *Journal of Experimental Botany* **66**: 4119–4131.

Yu H, Soler M, San Clemente H, Mila I, Paiva JA, Myburg AA, Bouzayen M, Grima-Pettenati J, Cassan-Wang H. 2015. Comprehensive genome-wide analysis of the *Aux/IAA* gene family in *Eucalyptus*: evidence for the role of *EgrIAA4* in wood formation. *Plant and Cell Physiology* **56**: 700–714.

Zhong R, McCarthy RL, Lee C, Ye ZH. 2011. Dissection of the transcriptional program regulating secondary wall biosynthesis during wood formation in poplar. *Plant Physiology* **157**: 1452–1468.

Zhu Y, Song D, Sun J, Wang X, Li L. 2013. *PtrHB7*, a class III HD-Zip gene, plays a critical role in regulation of vascular cambium differentiation in Populus. *Molecular Plant* **6**: 1331–1343.

Supporting Information

Additional Supporting Information may be found online in the Supporting Information section at the end of the article.

Dataset S1 Differentially expressed genes in the RNAseq-based transcriptomic analysis of *PtoIAA9m*-OE vs WT.

Fig. S1 Phylogenetic relationship of poplar and Arabidopsis *Aux/IAA* family members.

Fig. S2 Expression levels and patterns of poplar *Aux/IAA* genes in wood-forming stem tissues.

Fig. S3 Sequence alignment of PtoIAA9, Arabidopsis IAA8/9 and tomato IAA9.

Fig. S4 Attributes of a typical Aux/IAA protein harbored by the IAA9 protein.

Fig. S5 Generation and stem phenotypes of *PtoIAA9m*-OE poplar lines.

Fig. S6 Sequence, expression and protein interactions of ARF5s in poplar.

Fig. S7 Constitutive expression of *PtoARF5* in the *PtoIAA9m*-OE lines.

Fig. S8 Comparative transcriptomic analysis of the *PtoIAA9m*-OE and WT lines via RNAseq.

Fig. S9 Regulation of the PtoIAA9/ARF5 module on *PtoHB7/8* promoter activities via effector–reporter tests using GUS as a reporter gene.

Fig. S10 Constitutive expression of *PtoHB7* in the *PtoIAA9m*-OE lines.

Fig. S11 Expression of some secondary xylem development-related genes in *PtoIAA9m*-OE, *PtoARF5.1*- and *PtoHB7*-complementing transgenic lines.

Methods S1 Experimental methods for Figures S4 and S8, including subcellular localization, protein stability assay and mRNA sequencing.

Table S1 Primer sequences used in this study.

Please note: Wiley Blackwell are not responsible for the content or functionality of any Supporting Information supplied by the authors. Any queries (other than missing material) should be directed to the *New Phytologist* Central Office.